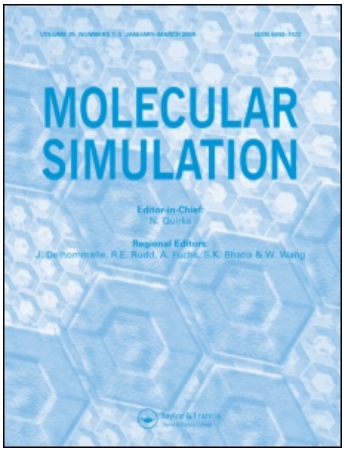

Molecular Simulation
Publication details, including instructions for authors and subscription information:
http://www.informaworld.com/smpp/title~content=t713644482

Combination of Neutron Scattering and Molecular Dynamics to Determine Internal Motions in Biomolecules

J. C. Smith[a]; G. R. Kneller[ab]
[a] Section de Biophysique des Prot'ines et des Membranes, D'partement de Biologie Cellulaire et Moléculaire, Centre Etudes Saclay, Gif-sur-Yvette, Cedex, France [b] IBM France, Paris, France

To cite this Article Smith, J. C. and Kneller, G. R.(1993) 'Combination of Neutron Scattering and Molecular Dynamics to Determine Internal Motions in Biomolecules', Molecular Simulation, 10: 2, 363 — 375
To link to this Article: DOI: 10.1080/08927029308022173
URL: http://dx.doi.org/10.1080/08927029308022173

Molecular Simulation, 1993, Vol. 10(2-6), pp. 363-375
Reprints available directly from the publisher
Photocopying permitted by license only

COMBINATION OF NEUTRON SCATTERING AND MOLECULAR DYNAMICS TO DETERMINE INTERNAL MOTIONS IN BIOMOLECULES

J.C. SMITH* and G.R. KNELLER[†,*]

**Section de Biophysique des Protéines et des Membranes, Département de Biologie Cellulaire et Moléculaire, Centre d'Etudes Saclay, 91191 Gif-sur-Yvette Cedex, France*
[†]IBM France, 68-76 Quai de la Rapée, F-75012 Paris, France.

(Received December 1992, accepted December 1992)

The forms and frequencies of atomic dynamics on the pico- and nanosecond timescales are accessible experimentally using incoherent neutron scattering. Molecular dynamics simulations cover the same space and time domains and neutron scattering intensities can be calculated from the simulations for direct comparison with experiment. To illustrate the complementarity of neutron scattering and molecular dynamics we examine measured and simulation-derived elastic incoherent scattering profiles from myoglobin and from the crystalline alanine dipeptide. Elastic incoherent scattering gives information on the geometry of the volume accessible to the atoms in the samples. The simulation-derived dipeptide elastic scattering profiles are in reasonable accord with experiment, deviations being due to the sampling limitations in the simulations and experimental detector normalisation procedures. The simulated dynamics is decomposed, revealing characteristic profiles due to rotational diffusional and translational vibrational motions of the methyl groups. In myoglobin, for which the timescale of the simulation matches more closely that accessible to the experiment, good agreement is seen for the elastic incoherent structure factor. This indicates that the space sampled by the hydrogen atoms in the protein on the timescale <100 ps is well represented by the simulation. Part of the helix atom fluctuations can be described in terms of rigid helix motions.

KEY WORDS: Molecular dynamics, incoherent neutron scattering, peptide crystals, myoglobin, diffusive motions

INTRODUCTION

Molecular dynamics is now a standard method for the investigation of pico- and nanosecond motions in condensed phase chemical and biological systems [1] [2]. In proteins, measurements using several experimental techniques indicate that motions exist on these timescales but few data have been available that allow a comparison with simulations of the types of dynamics involved and their geometries. Information on time-dependent self-correlations of atoms can be gained from incoherent neutron scattering [3] [4] [5]. Measured neutron scattering spectra are a sum of scattering intensities from single atoms. The spectra are recorded as a function of the energy transfer, ω and momentum transfer, $\vec{q}$ between the neutrons and the sample. Neutrons are excellent dynamical probes because the experimentally-accessible ranges of ω and $\vec{q}$ correspond to the typical timescales (*ps*, *ns*) and amplitudes (Å) of atomic motions.

The basic quantity measured in incoherent neutron scattering is $\mathscr{S}_{\text{inc}}(\vec{q}, \omega)$, the incoherent dynamic structure factor. The incoherent dynamic structure factor is written as

$$\mathscr{S}_{\text{inc}}(\vec{q}, \omega) = \frac{1}{2\pi} \int_{-\infty}^{+\infty} dt\, e^{-i\omega t} \mathscr{F}_{\text{inc}}(\vec{q}, t) \tag{1}$$

$$\mathscr{F}_{\text{inc}}(\vec{q}, t) = \frac{1}{N} \sum_{\alpha} b_{\alpha,\text{inc}}^2 \left\langle e^{-i\vec{q}\cdot\vec{\mathbf{R}}_\alpha(0)} e^{i\vec{q}\cdot\vec{\mathbf{R}}_\alpha(t)} \right\rangle \tag{2}$$

We see from Equation 1 that $\mathscr{S}_{\text{inc}}(\vec{q}, \omega)$ is the time Fourier transform of a time correlation function, $\mathscr{F}_{\text{inc}}(\vec{q}, t)$ which is called the incoherent intermediate scattering function. The sum in Equation 2 is over the N atoms, α in the sample. The vector operators $\vec{\mathbf{R}}_\alpha(t)$ denote the atomic position operators. They are replaced by normal position vectors if $\mathscr{F}_{\text{inc}}(\vec{q}, t)$ is calculated as a classical time correlation function.

To each atom belongs an incoherent scattering length $b_{\alpha,\text{inc}} \doteq \sqrt{\overline{b_\alpha^2} - \overline{b_\alpha}^2}$. It is defined as the RMS fluctuation of the scattering length b_α. b_α defines the strength of the nucleus-neutron interaction and depends on the isotope of the nucleus and the relative orientation of the neutron spin with respect to the spin of the nucleus. $b_{\alpha,\text{inc}}$ for hydrogen is much larger than any other (incoherent or coherent) scattering length. Therefore in most organic molecules, which contain typically 50% hydrogen atoms, incoherent scattering from these atoms dominates the measured intensities. In the following we take only hydrogen atoms into account and use a renormalized scattering length $b_{H,\text{inc}} = 1$. The subscript 'inc' is dropped since we deal only with incoherent scattering.

Incoherent scattering can be classified as three types: elastic, quasielastic and inelastic. The inelastic scattering arises from vibrational motion in the sample. Quasielastic scattering manifests as a broadening of the elastic peak and indicates the presence of nonvibrational, diffusive motions in the sample [4]. Inelastic scattering and quasielastic scattering are discussed elsewhere for the dipeptide [11] and proteins [5]. In this article we examine the elastic scattering. Decomposing $\mathscr{F}(\vec{q}, t)$ into time-independent and time-dependent parts gives

$$\mathscr{F}(\vec{q}, t) = \text{EISF}(\vec{q}) + \mathscr{F}'(\vec{q}, t), \tag{3}$$

$$\text{EISF}(\vec{q}) = \lim_{t \to \infty} \mathscr{F}(\vec{q}, t), \tag{4}$$

where EISF stands for **E**lastic **I**ncoherent **S**tructure **F**actor. We have

$$\mathscr{S}(\vec{q}, \omega) = \text{EISF}(\vec{q})\delta(\omega) + \mathscr{S}'(\vec{q}, \omega). \tag{5}$$

As is evident from Equation 5 the EISF describes the *elastic* scattering with zero energy transfer ($\omega = 0$). It follows from the definition of the EISF in Equation 4 that

$$\text{EISF}(\vec{q}) = \frac{1}{N} \sum_{\alpha} \left| \left\langle e^{i\vec{q}\cdot\vec{R}_\alpha} \right\rangle \right|^2. \tag{6}$$

Using Equation 6 the EISF($\vec{q}$) can be calculated from molecular dynamics trajectories as a static time average, enabling a direct comparison between experiment and simulation.

The EISF is determined by the volume explored by the hydrogen atoms. This can be seen by introducing the van Hove selfcorrelation function $\mathcal{G}_s(\vec{r}, t)$ [6]:

$$\mathcal{G}_s(\vec{r}, t) \doteq \int d^3q\, e^{-i\vec{q}\cdot\vec{r}} \mathcal{F}(\vec{q}, t). \tag{7}$$

$\mathcal{G}_s(\vec{r}, t)d^3r$ is the probability of finding an (hydrogen) atom in a volume element d^3r around the position $\vec{r}$ at time t, given that it was at $\vec{r} = 0$ at $t = 0$. From the definition in Equation 7 it follows that

$$\mathrm{EISF}(q) = \frac{1}{2\pi^3} \int d^3r\, e^{i\vec{q}\cdot\vec{r}} \mathcal{G}_s(\vec{r}, \infty), \tag{8}$$

i.e. the EISF is the spatial Fourier transform of the long time limit of $\mathcal{G}_s(\vec{r}, t)$. For systems like liquids, in which the motions of the atoms are unconstrained, the long time limit of $\mathcal{G}_s(\vec{r}, t)$ approaches $1/V$, where V is the infinite volume of the accessible space, and the EISF vanishes. The EISF is finite only for systems in which the atomic motions are confined to some part of the configurational space.

In previous protein work quasielastic and inelastic (vibrational) scattering profiles were measured, calculated from simulations and compared [5] [7] [8] [9] [10]. Here we analyse the geometries of the hydrogen motions in the crystalline alanine dipeptide and in myoglobin. In the alanine dipeptide, (CH_3-CONH-$C_\alpha H(C_\beta H_3)$-CONH-CH_3) the neutrons probe essentially the dynamics of the three methyl groups in the molecule. The side-chain methyl has an intrinsic (gas-phase) barrier of ~3 kcals/mol whereas the N-ter and C-ter methyls have much smaller intrinsic barriers, ~0 kcals/mol [11]. We loosely refer to these as the 'hindered' and 'free' methyls. These terms refer to the intrinsic barrier; in the crystal an effective rotational barrier will exist for all methyls due to the influence of nonbonded interactions.

The 300 K dynamics of myoglobin contains vibrational and diffusive components [5] [8]. The diffusive motions may be essential to the correct functioning of globular proteins [12]. Incoherent neutron scattering experiments have demonstrated that at least some of the diffusive motions occur on a picosecond-nanosecond timescale [7] [13]; Moessbauer spectroscopy suggests that slower motions may also be involved [14]. A detailed characterization of the nature of the diffusive motions has not yet been made. A model for the hydrogen motions based on jumps on an asymmetric two-state potential was initially suggested [13] and an analysis based on mode-coupling theory has also been reported [15]. Molecular dynamics simulations of myoglobin reproduce reasonably well the temperature-dependence of the measured incoherent neutron scattering spectra [5] [8] [16].

In the work presented here we compare experimental and simulated elastic incoherent structure factors for the alanine dipeptide and myoglobin. Differences are rationalised in terms of the way the experimental data was reduced or sampling limitations in the simulations–some significant differences are seen in the dipeptide case. The dipeptide trajectories are decomposed so as to identify simple dynamical characteristics contributing to the observed scattering. For the dipeptide we separate contributions to the scattering due to the rotational and translational dynamics of the methyl groups. The EISF(q) derived from the 100 ps myoglobin trajectory is in excellent agreement with experiment. We examine the contribution of rigid-helix motions to the full molecular dynamics trajectory.

The combined neutron-simulation approach is a means to define the essential characteristics of the internal dynamics of biomolecules. In the dynamically heterogeneous systems studied here direct interpretation of the experimental data with simple analytical models can be difficult and dangerous. Molecular dynamics can make a reliable connection between experiment and theory; certain types of motion present as components of the simulated trajectories but obscured in the experimental profiles can be identified, abstracted and mapped onto analytical descriptions such as those of harmonic or damped harmonic vibrations, jump diffusion or continuous diffusion along geometric paths. Conversely, the comparison between experiment and simulation can provide insights into how to improve the simulation methodology and potential functions and into how data reduction and collection procedures can influence the experimental scattering profiles.

METHODS

Details of the dipeptide experiments and simulations [11] and of the myoglobin simulations [19] [20] are presented elsewhere and will therefore be only outlined here.

The dipeptide neutron scattering experiments were performed on polycrystalline samples of the alanine dipeptide on the backscattering spectrometer IN13 at the Institut Laue-Langevin, Grenoble. The myoglobin experimental data, measured on IN13 and on a time-of-flight spectrometer, IN6 were taken from the literature [13].

The simulations were performed in the microcanonical ensemble using the program CHARMM [17]. The alanine dipeptide was simulated including the full crystal environment using periodic boundary conditions. The primary box was chosen to be that of two unit cells, consisting of of 16 dipeptide molecules i.e., 352 atoms. Simulations were performed at 50 K, 100 K and 300 K for 20 ps. Myoglobin was simulated without explicit solvent for 100 ps. The simulation and three-dimensional structure of the protein were stable.

The simulation analysis was performed with the program package *n*MOLDYN [18]. The EISF was calculated from the atomic trajectories using Eq. 6. The trajectories were further analysed in terms of rigid body motions by fitting rigid reference structures to each trajectory frame (methyl groups for the dipeptide and helices for myoglobin) using a general method for the optimal superposition of molecular structures [21].

RESULTS

We focus our analysis on the elastic incoherent structure factors. In certain respects the information contained in the EISF is similar to that obtained for heavy atoms from X-ray crystallographic temperature factors. Information is lost compared to the X-ray case insofar as the EISF is an *average* over the atoms in the system. However, several important advantages exist. The neutron EISFs are *single particle* properties and do not contain a complicating static disorder contribution due to coherent scattering. Direct comparison with molecular dynamics is thus justifiable. In addition, there is no need to assume any particular type of dynamics (e.g., isotropic, harmonic) to interpret the results. Finally, as will be illustrated, the EISFs are very sensitive quantities and mean-square fluctuation differences of ~ 0.01 Å^2 can be distinguished.

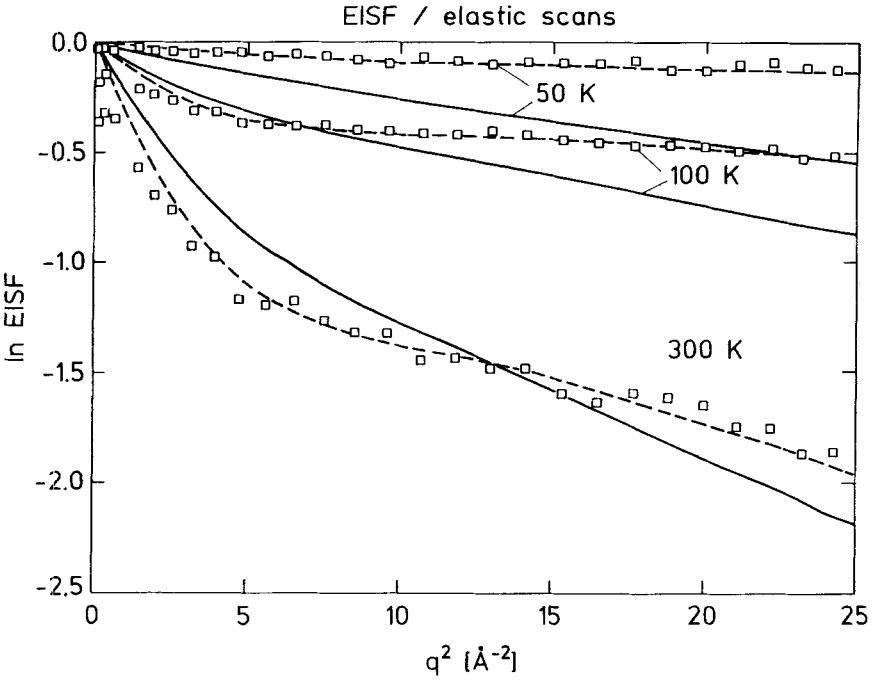

Figure 1 Log of the elastic intensity versus q^2 for the alanine dipeptide in crystalline form from the IN13 experiment (squares), the simulations (solid lines) and using the correction formula (Equation 11). The values of p, the population factor are 0 at 50 K, 0.15 at 100 K and 0.35 at 300 K. The corresponding values for the subtracted vibrational RMS displacements are 0.130 Å at 50 K, 0.133 Å at 100 K and 0.140 Å at 300 K. For more details see reference [11].

Methyl group dynamics in the alanine dipeptide

To determine the significance of the measured and simulated EISF(q) curves one must consider a number of different influences such as those due to the instrumental resolution and data reduction and to the simulation methodology. Any decrease of the experimental EISFs with q from their normalised maximum value indicates the presence of hydrogen atom motions in the sample on the timescale of the instrumental resolution (~500 ps or faster for IN13). The form of EISF(q) versus q is determined by the type of dynamics present. For example, a linear decrease of lnEISF(q) with q^2 i.e., a Gaussian dependence on q, results from certain types of dynamics such as harmonic or damped harmonic motion [3]. NonGaussian behaviour can be described in terms of other processes such as activated jumps between conformational substates [4] [13].

Dipeptide simulation-derived and experimental EISF(q)

In Figure 1 is shown the experimental q-dependence of the elastic scattering from the dipeptide crystal. Also shown is the EISF(q) derived from the simulations. At 300 K

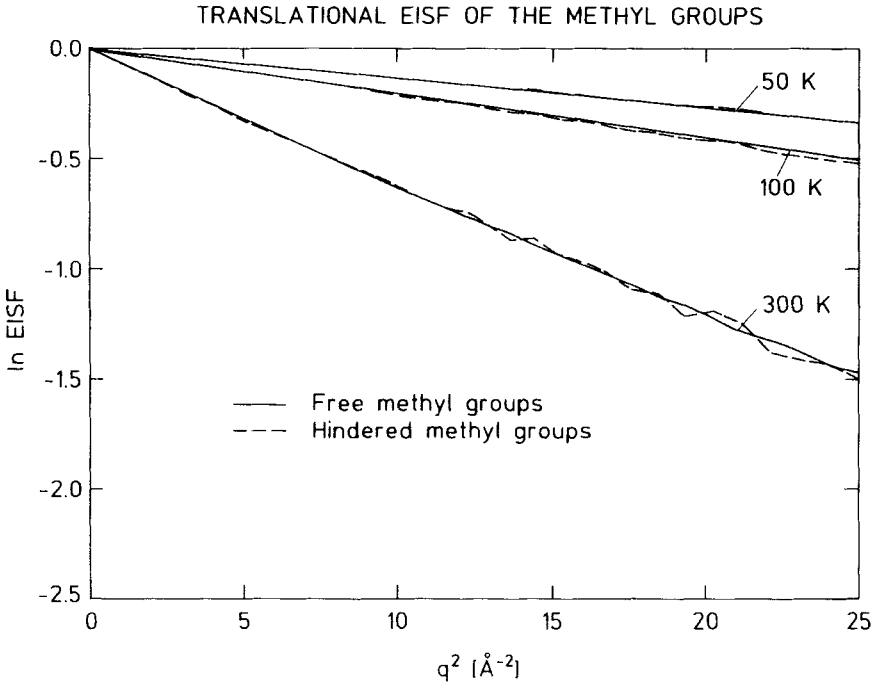

Figure 2a

in both experiment and simulation the EISF(q) is strongly nonGaussian with a fast-decreasing component at low q followed by a more linear region between 6 $Å^{-2}$ and 25 $Å^{-2}$. Nonlinearity is also seen in the 100 K data, although less apparent in both the simulation and experimental curves. At 50 K both curves are almost linear, consistent with the presence of essentially vibrational motion at this temperature.

Translational and rotational methyl components

Before discussing the differences between the experimental and simulation-derived elastic scattering in Figure 1 we decompose the simulation-derived contributions using the rigid body analysis. In Figure 2a is shown the contribution to the elastic scattering from the translational motion of the free and hindered methyl groups. The hindered and free groups present almost identical translational elastic scattering, Gaussian in q^2, arising from purely vibrational motion. In Figure 2b is presented the equivalent rotational contribution. For the free groups nonGaussian behaviour is clear at all temperatures. At 300 K a minimum is seen at 9 $Å^{-2}$ and a subsidiary maximum at 15 $Å^{-2}$. The form of the rotational curve at 300 K is close to that of the spherical Bessel function found by analytical solution for the elastic scattering from certain models for methyl rotational dynamics [4]. Further examination shows that the 300 K rotational curve is not consistent with a 3-site jump model, for which the minimum occurs at lower q values, but rather with a

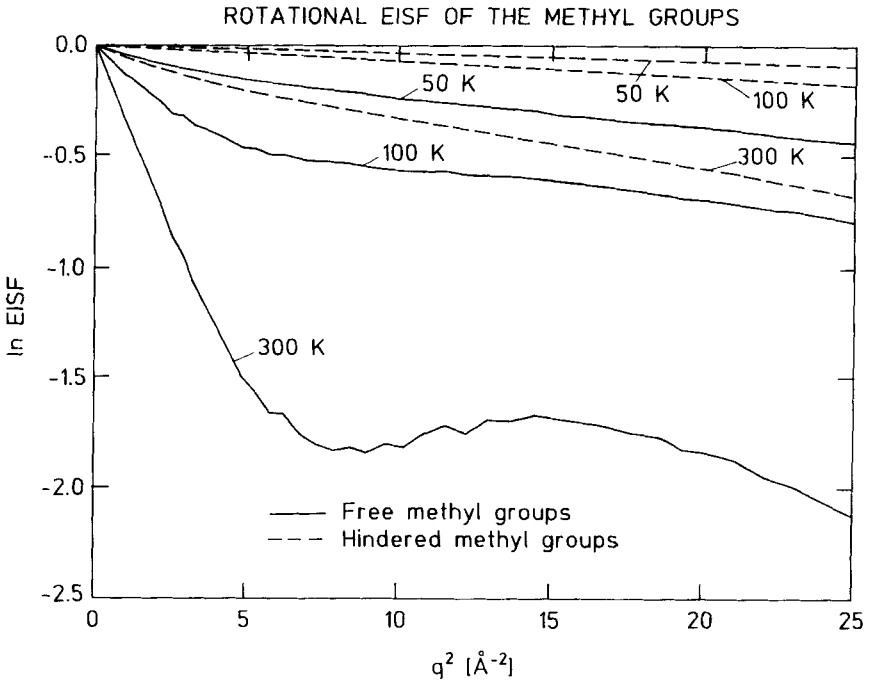

Figure 2 Decomposition of the simulation-derived alanine dipeptide EISF(q). a) translational component b) rotational component.

jump model with multiples of 3 sites or continuous diffusion on a circle. This is in accord with the qualitative behaviour of the angular rotational time series for the free methyls [11] (not shown). The hindered groups in Figure 2b have a relatively weak q-dependence with some nonlinearity. This reflects the fact that jump-diffusive hindered methyl rotational dynamics is not fully developed in the simulations.

Determining the EISF from experiment and simulation

It is worthwhile to discuss the effects of instrumental resolution and of insufficient sampling in the simulations. The EISFs from the simulations are calculated directly as a *time average* i.e.,

$$\mathrm{EISF}(\vec{q}) = \lim_{T\to\infty} \frac{1}{N} \sum_{\alpha} \frac{1}{T} \int_0^T d\tau \left| \langle e^{i\vec{q}\cdot\vec{R}_\alpha} \rangle \right|^2, \tag{9}$$

making the assumption that

$$\lim_{T\to\infty} \frac{1}{T} \int_0^T d\tau \ldots \approx \frac{1}{T_{md}} \int_0^{T_{md}} d\tau \ldots \tag{10}$$

where T_{md} is the simulation length.

In the experiment one has a different problem, that of extracting a well-sampled

EISF in the *frequency domain*. All processes that are slower than $T_{exp} = \frac{1}{\Delta\nu_{res}}$, where $\Delta\nu_{res}$ is the instrumental resolution, are recorded as elastic scattering. T_{md} should therefore not be confused with or directly equated with T_{exp}.

Low q differences between experiment and simulation

At low q the experimentally-derived higher temperature elastic scattering is less intense than in the simulation. The slope of log EISF as $q \to 0$ gives the mean-square displacement in the long time limit [3]. Figure 1 therefore implies that the simulation-derived mean-square displacements are smaller than the experimental values. The difference in the 300 K dipeptide experimental and simulation-derived EISF(q) at low q are possibly due to rotational transitions of the methyl groups that are resolvable by the experiment but poorly sampled in the simulation.

High q difference between experiment and simulation

The difference at high q is the inverse of that at low q; for all temperatures the experimentally-derived elastic scattering in Figure 1 is more intense than that derived from the simulations. The fact that, at high q, log EISF is close to linear in the simulations and experiments, together with the fact that log EISF_{sim} < log EISF_{exp}, suggests that the simulation-derived vibrational amplitudes are larger than those contributing to the experimental elastic scans. The difference in the vibrational dynamics not evidently explicable at first sight, especially when the 50 K scattering is considered. At 50 K the difference between simulation and experiment is quite considerable and yet the simulated vibrations should not suffer from the sampling problem. Moreover, the modification of the vibrational amplitudes due to quantum-mechanical effects is small.

To appreciate the magnitude of the apparent discrepancy we note that the effect on the high-q EISF of a small change in the vibrational mean-square displacements is dramatic; a difference of only ≈ 0.02 Å^2 in the mean square fluctuation (5% of the 300 K vibrational mean square fluctuation in Figure 1) corresponds to a difference of 0.5 in log EISF at $q = 5$ Å^{-1}. This is a small effect at 300 K and implies that the EISF curves are highly sensitive.

Matching experimental and simulation data

One can summarize the above considerations formally in the following 'correction formula' for the EISF, designed to approximately correct for over- and under-estimation of motions in the simulations:

$$\text{EISF}(q) = \text{EISF}_{sim}(q) \cdot \frac{\text{EISF}_+(q)}{\text{EISF}_-(q)}. \tag{11}$$

$\text{EISF}_+(q)$ is the EISF due to rotational motion to be added to the simulation trajectory and $\text{EISF}_-(q)$ the EISF due to the vibrational motion to be subtracted from the simulation;

$$\text{EISF}_+(q) = 1 - p(1 - A_0(q)), \tag{12}$$

$$\text{EISF}_{-}(q) = e^{-q^2\langle u_\Delta^2\rangle}. \tag{13}$$

In Equation 12 p is the fraction of methyl groups not showing rotational transitions in the simulation that are seen in the experiment. $A_0(q)$ is the EISF of the additional rotational motion. For a rotational jump model this is typically a linear combination of zeroth-order spherical Bessel functions depending on the jump model assumed [4]; which model is taken is not important since only the general behaviour counts here. In Equation 13 $\langle u_\Delta^2\rangle$ denotes the vibrational mean-square fluctuation to be subtracted. In Figure 1 the dashed lines show the corrected EISF using the simple model described above. The parameters p and $\langle u_\Delta^2\rangle$ are given in the figure caption. p increases with T whereas $\langle u_\Delta^2\rangle$ remains constant.

That $\langle u_\Delta^2\rangle$ is small and constant with T immediately suggests some small systematic difference in the vibrational contribution. Indeed, a strong candidate for this can be finally identified in the experimental data reduction procedure. To calibrate the neutron detectors it was necessary to normalise all the measured scattering to that at 22 K. This removes the decay of the EISF due to the 22 K vibrations, leading to an underestimation of the experimental vibrational mean square fluctuations at higher temperatures. Whereas this effect becomes small at 300 K, it leads to a significant discrepancy at 50 K. Thus it appears that the high q difference between experiment and theory can be mostly attributed to the experimental detector normalisation procedure.

Myoglobin

In Figure 3 a comparison is made between the measured and simulated elastic scattering for myoglobin. In both experiment and simulation a non-Gaussian form is seen for the elastic scattering. The calculated EISF is in excellent agreement with experiment. In a previous analysis from a 125 ps trajectory it was demonstrated that, due to heterogeneity in the hydrogen atom mean square displacements, the observed elastic scattering can be non-Gaussian even when the contributions from individual hydrogens are Gaussian [8]. However, quantitative agreement with agreement with experiment was not achieved. In the present case, the absence of the Gaussian approximation (Equation 6 was used directly to calculate the EISF) results in improved, quantitative agreement with experiment, as seen in Figure 3. The low q behaviour indicates that the mean square displacements are still slightly underestimated in the simulation; the low q 300 K scattering matches that experimentally obtained at 277 K. This can be attributed to the fact that the hydrogen motions contributing to the experimental profile are not quite completely sampled in the simulation. However, the overall agreement between experiment and simulation indicates that the amplitudes of the vibrational and diffusive motions of myoglobin are well represented in the simulations over the accessible timescale, 0–100 ps.

As the amplitudes of the simulated dynamics are in good agreement with experiment it will be of interest to try to identify from the *simulations* the nature of the diffusive motions concerned. The question therefore arises as to whether the full atomic trajectories can be simply described. How to do this is not trivial. We have employed the rigid-body analysis method to to fit rigid helices to each to the simulation timeframes [20]. The residue-dependence of the main chain atom fluctuations derived from the rigid helix trajectories is shown in Figure 4 together with the full trajectory results. The RMS atomic fluctuation averaged over all the

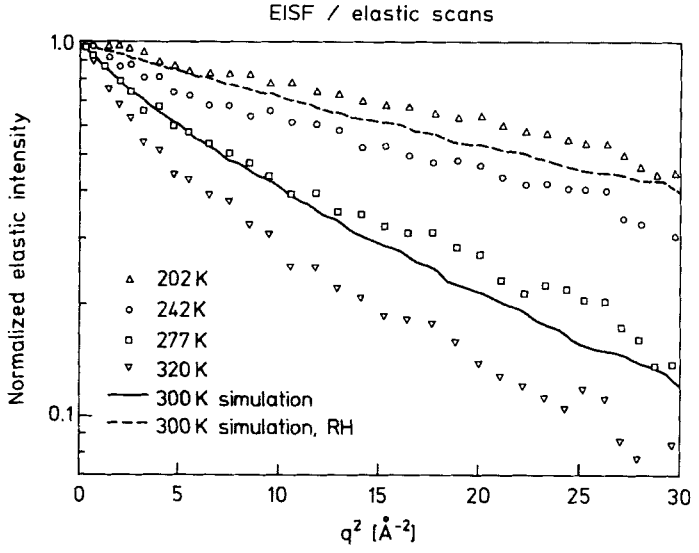

Figure 3 Log of the elastic intensity versus q^2 for myoglobin. The experimental values are taken from reference [13] at $T = 202$ K (triangles, tip up), $T = 242$ K (circles), $T = 272$ K (squares), $T = 320$ K (triangles, tip down). The 300 K simulation-derived EISF(q) is 21 given as a solid line and the rigid-helix contribution as a dashed line.

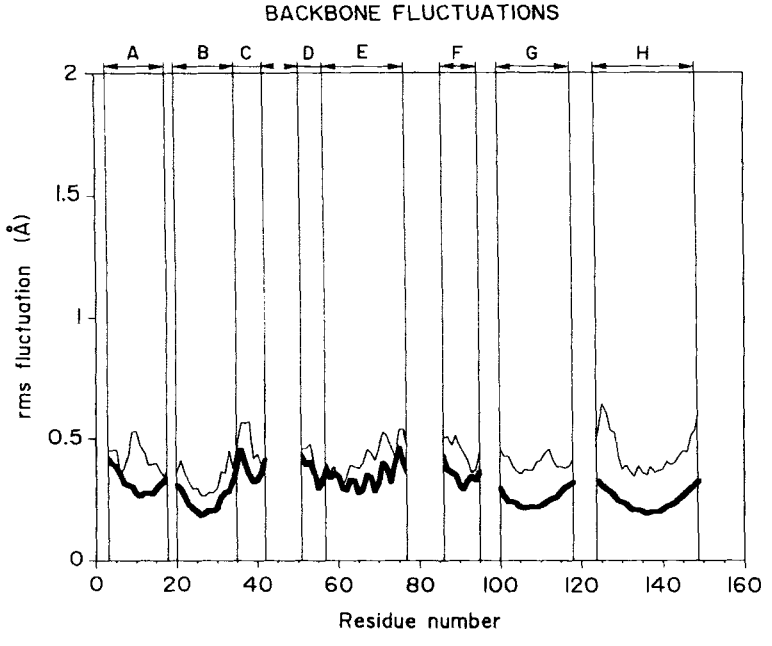

Figure 4 Residue-dependence of the RMS atomic fluctuations for the helix backbone atoms of the full trajectory (thin line) and the rigid-helix trajectory (thick line) of myoglobin.

atoms of all the helices is 0.31 Å in the rigid-helix trajectory compared to 0.53 Å in the full trajectory. Thus about 60% of the helix atom fluctuations can be described by the rigid-helix dynamics. This result indicates that there is a significant contribution from the fluctuations of the helix atoms around the rigid helix configurations. In the full trajectory (Figure 4, thin line) several helices (B, F, G, H) exhibit the characteristic that the fluctuation magnitudes of the backbone atoms tend to be smaller in the central part of the helix than in the extremeties. This tendency is also seen in the rigid-helix trajectories and can be attributed to rotational rigid-body motion about one or other of the two axes passing through the centre of mass of the helix and perpendicular to the helix axis. Helix E shows oscillations in the fluctuation distribution corresponding to the helix pitch.

The contribution of the rigid-helix motions to the measured EISFs can be assessed by calulating the EISF from the rigid-helix trajectory. This is shown as the dashed line in Figure 3. The rigid-helix EISF falls off more slowly than the full trajectory or experimental EISFs. This confirms that in the long and short time domains rigid-helix motions contribute only partially to the exploration by the hydrogen atoms of their accessible volume.

CONCLUSIONS

The properties of the neutron are such that the experimentally-accessible time and space domains correspond to the distances and timescales of atomic motions sampled in MD simulations. This together with the simplicity of the neutron-nucleus interaction makes incoherent neutron scattering a unique tool for the analysis of picosecond timescale hydrogen atom motions and enables a direct comparison between the simulation-derived and experimental spectra.

The measured elastic incoherent structure factor is determined by the geometry of the space explored by the moving protons within the timescale determined by the instrumental energy resolution. It is thus useful in determining whether the forms and amplitudes of the hydrogen displacements are correctly represented in the simulations. In the work presented here we have examined the hydrogen atom motions present in the alanine dipeptide and in myoglobin. The simulation-derived and experimental EISFs are generally in good agreement, more so for myoglobin where the length of the simulation reduces the configurational sampling insufficiency. For both systems the good agreement between experiment and simulation gives us confidence to go further and analyse the simulations in terms of different types of motion contributing to the atomic displacements and to the neutron spectra.

Simulations can provide a stepping stone between experiment and analytical theory. This has not been necessary for some molecular systems simpler than those studied here in which the measured EISF(q) can be unambiguously attributed to dynamical behaviour described by analytical theory [4]. However, in the alanine dipeptide and myoglobin the dynamics is too complicated and the resulting experimental EISF(q)s are not readily directly interpretable. In the case of the dipeptide simply interpretable scattering profiles are found if one examines the translational and rotational *components* of the trajectories of the free and hindered methyl groups.

In myoglobin, the diffusive motions leading to the nonGaussian EISF(q) are frozen in over the picosecond timescale at low temperatures [5] [13]. It may be

suggested that it is these motions that are necessary for the functioning of proteins [12] [22]. As the amplitudes of the simulated dynamics are in good agreement with experiment it will be of interest to try to identify from the *simulations* the nature of the diffusive motions concerned. Rigid helix motions contribute part of the helix atom mean square fluctuations. A detailed analysis of the fitted rigid-body trajectories in terms of fluctuations, mean-square displacements, velocity correlation functions and vibrational frequency distributions has been made [19]. Further work is underway with a view to obtaining an improved simple description of the atomic displacements that dominate the helix and side-chain dynamics.

Acknowledgements

We acknowledge IBM France and the Commissariat á l'Energie Atomique for financial support and for use of supercomputing facilities. We thank the Institut Laue-Langevin for the use of their neutron scattering facilities and Dr. W. Petry for help with the experiments. The alanine dipeptide experiments were performed in collaboration with Drs. Wolfgang Doster and Stephen Cusack. The myoglobin calculations were performed in collaboration with Dr. Sylvie Furois-Corbin.

References

[1] W.F. van Gunsteren & H. Berendsen, 'Computer Simulation of Molecular Dynamics: Methodology, Application and Perspectives in Chemistry' *Angew. Chem. Int. Ed. Engl.* **29**, 992-1023 (1990).

[2] C.L. III Brooks, M. Karplus, & B.M. Pettitt, Proteins. A Theoretical Perspective of Dynamics, Structure and Thermodynamics. *Adv. Chem. Physics* **71** (Eds. I. Prigogine & S. Rice). Wiley. (1988).

[3] S. Lovesey, *Theory of Neutron Scattering from Condensed Matter*. International Series of Monographs on Physics, no. 72 Oxford Science Publications. Oxford:Clarendon, (1984).

[4] M. Bee. *Quasielastic Neutron Scattering: Principles and Applications in Solid State Chemistry, Biology and Materials Science*. Bristol and Philadelphia: Adam Hilger (1988).

[5] J.C. Smith, Protein Dynamics: Comparison of Simulations with Inelastic Neutron Scattering Experiments. *Q. Rev. Biophys.* **24(3)**, 227-291 (1991).

[6] L. Van Hove, Correlations in Space and Time and Born Approximation Scattering in Systems of Interacting Particles. *Phys. Rev.* **95(1)**, 249-262 (1954).

[7] J.C. Smith, S. Cusack, B. Tidor and M. Karplus, Inelastic Neutron Scattering Analysis of Low Frequency Motions in Proteins: Harmonic and Damped Harmonic Models of the Bovine Pancreatic Trypsin Inhibitor, *J. Chem. Phys.* **93(5)**, 2974-2991 (1990).

[8] J.C. Smith, K. Kuczera & M. Karplus, Dynamics of Myoglobin: Comparison of Simulation Results with Neutron Scattering Spectra. *Proc. Natl. Acad. Sci.* (U.S.A.) **87**, 1601-1605 (1990).

[9] S. Cusack, J.C. Smith, J.L. Finney, B. Tidor & M. Karplus, Inelastic Neutron Scattering Analysis of Picosecond Internal Protein Dynamics. Comparison of Harmonic Theory with Experiment. *J. Mol. Biol.* **202**, 903-908 (1988).

[10] E. Clementi, G. Corongiu, M. Aida, V. Niesar & G.R. Kneller, Monte Carlo and Molecular Dynamics Simulations. In *Modern Techniques in Computational Chemistry* (Ed. E. Clementi) Escom: Leiden (1990).

[11] G.R. Kneller, W. Doster, M. Settles, S.C. Cusack and J.C. Smith, *J. Chem. Phys.* In Press.

[12] B.F. Rasmussen, A.M. Stock, D. Ringe & G.A. Petsko, Crystalline ribonuclease A loses function below the dynamical transition at 220 K. *Nature* **357**, 423-424 (1992).

[13] W. Doster, S. Cusack & W. Petry, Dynamical Transition of Myoglobin Revealed by Inelastic Neutron Scattering. *Nature* **337**, 754-756 (1989).

[14] E.W. Knapp, S.F. Fischer & F. Parak, Protein Dynamics from Moessbauer Spectra. The Temperature Dependence. *J. Chem. Phys.* **78(7)**, 4701-4711 (1983).

[15] S. Cusack & W. Doster, Temperature Dependence of the Low-Frequency Dynamics of Myoglobin. Measurement of the Vibrational Frequency Distribution using Inelastic Neutron Scattering. *Biophys. J.* **58**, 243-251. (1990).
[16] R.J. Loncharich & B. Brooks, Temperature Dependence of the Dynamics of Hydrated Myoglobin. Comparison of Force Field Calculations with Neutron Scattering Data. *J. Mol. Biol.* **215**, 439-455, (1990).
[17] B. Brooks, R. Bruccoleri, B. Olafson, D. States, S. Swaminathan & M. Karplus, CHARMM. A program for Macromolecular Energy, Minimisation and Dynamics Calculations. *J. Comp. Chem.* **4**, 187-217, (1983).
[18] G.R. Kneller, nMOLDYN. A Program for Calculation of Neutron Scattering Intensitites from Molecular Dynamics Simulations. To be published.
[19] S. Furois-Corbin, J.C. Smith & G.R. Kneller, Proteins: *Struct., Funct., Genetics.* In Press.
[20] S. Furois, G.R. Kneller & J.C. Smith. Protein Simulations Using Supercomputers. *Jornades de Supercomputació a Catalunya, CATSUPERCOMP* 103-110 (1992) Fundació Catalana per a la Recerca.
[21] G.R. Kneller. Superposition of Molecular Structures Using Quaternions. *Molecular Simulation* **7**, 113-119, (1991).
[22] M. Ferrand. Etude des Mouvements Internes de la Bacteriorhodopsine par Diffusion Inelastique des Neutrons et Simulation de Dynamique Moléculaire. *Thèse de Doctorat* Université de Grenoble (1991).